Chalcogenide Letters Vol. 13, No. 12, December 2016, p. 555 - 562

SOLVOTHERMAL SYNTHESIS OF $CuCo_2S_4$ NANOPARTICLES FOR RECHARGEABLE LITHIUM-ION BATTERY ANODES

L.NIE[a], H.WANG[a], S.LIU[b,c*], R.YUAN[a]
[a]*Key Laboratory of Luminescent and Real-Time Analytical Chemistry (Southwest University), Ministry of Education, College of Chemistry and Chemical Engineering, Southwest University, Chongqing 400715, China*
[b]*Institute of Chemical Materials, China Academy of Engineering Physics, PO Box 919-301, Mianyang 621900, P. R. China*
[c]*Sichuan Research Center of New Materials, 596 Yinhe Road, Shuangliu district, Chengdu 610200, China*

Ternary $CuCo_2S_4$ nanoparticles were synthesized *via* a solvo thermal method using metal acetates and thiourea as starting materials.The as-prepared samples, which were agglomerated by irregular nanoparticles, exhibited a cubic-phase, polycrystalline structure with an average crystallite size of 15.8 nm. As an anode material for rechargeable lithium-ion batteries, $CuCo_2S_4$ nanoparticles exhibited a high specific capacity of 1166.2 mAh g^{-1} at a current density of 100 mA g^{-1} after 160 cycles.

(Received November 8, 2016; Accepted December 16, 2016)

Keywords: Solvothermal; $CuCo_2S_4$; Nanoparticles; Anode materials; Lithium-ion batteries

1. Introduction

Due to low toxicity, relative cheapness, abundance in nature, high specific capacity,as well as excellent electrochemical performance, copper or cobalt based sulfides are presently researched as promising electrode materials for lithium ion batteries (LIBs),[1] such as binary copper sulfides Cu_xS_y[2-6] and cobalt sulfides Co_xS_y,[7-12] ternary copper tin sulfide Cu_2SnS_3[13]and nickel cobalt sulfide $NiCo_2S_4$,[14]as well as quaternary copper indium zinc sulfideCuInZnS[15] and copper zinc tin sulfide Cu_2ZnSnS_4,[16]*etc*.

It is generally believed that ternary sulfides can offer higher electrical conductivity and richer redox chemistry than binary sulfides, as well as combine their contributions from both metal ions.[14, 17] For instance, ternary Cu_2SnS_3 cabbage-like nanostructures deliver a good specific capacity of 621 mAh g^{-1} at 100 mA g^{-1} after 50 cycles;[13] ternary $NiCo_2S_4$ hollow spheres exhibit a high specific capacity of 696 mAh g^{-1} at a current density of 200 mA g^{-1} after 100 cycles.[14] It is also reported that cobalt sulfides have a good thermal stability and a high theoretical lithium storage capacity (870 mAh g^{-1} for CoS_2, which is higher than 372 mAh g^{-1} for commercial graphite).[18] In addition, copper sulfides have a high electrical conductivity (10^{-3} S cm^{-1} for CuS) which is beneficial for enhancing the electrochemical performance of anode materials.[6] Therefore, synthesis and electrochemical measurements of nanostructured ternary sulfides which possess merits of both copper sulfides and cobalt sulfides are expected for promising LIB anode materials. Very recently, $CuCo_2S_4$ nanomaterials are extensively reported for high-performance supercapacitors, such as nanoparticles,[19] hollow nanoneedle arrays,[20] and $CuCo_2S_4$/CNT/graphene nanocomposite.[21] Also, our group has just investigated flower-like $CuCo_2S_4$ nanosheets/graphene composites with enhanced lithium storage properties.[22] However,

*Corresponding author: sliu@caep.cn

understanding of the pristine copper cobalt sulfide nanomaterials as an anode material for the rechargeable lithium-ion batteries is still limited.

In this work, ternary copper cobalt sulfide $CuCo_2S_4$nanoparticles were synthesized by a one-pot solvothermal method.Crystal structures, morphologies, microstructures and compositions of the as-prepared $CuCo_2S_4$ nanoparticles were characterized by X-ray diffraction (XRD), scanning electron microscopy (SEM), transmission electron microscopy(TEM), X-ray photoelectron spectroscopy (XPS), *etc*. Lastly, the electrochemical properties of such anode materials for LIBs were investigated in detail.

2. Experimental section

2.1 Preparation of $CuCo_2S_4$ nanoparticles

All the chemicals were of analytical grade. Firstly, 1mmol of copper acetate $Cu(CH_3COO)_2{\cdot}H_2O$, 2 mmol of cobalt acetate $Co(CH_3COO)_2{\cdot}4H_2O$ and 4 mmol of thiourea$(NH_2)_2CS$ were separately dissolved in 20 ml of ethyl glycol under stirring for 10 min. Secondly, the above solutions were mixed under stirring. Thirdly, the mixed solution was transferred to a Teflon-lined stainless steel autoclave and heated in an electric oven at 200 ºC for 12 h. Once reaction, the autoclave was cooled down to the room temperature. Finally, black powders were collected by centrifugation, washed with di-ionized water and absolute alcohol thoroughly, and then dried under vacuum at 70 ºC for 12 h for further characterizations.

2.2 Characterizations

Powder XRD patterns were collected using a MaXima-7000 (Shimadzu, Japan) diffractometer with graphite-monochromatized Cu *Kα* radiation (*λ*= 1.5418 Å).SEM images and energy-dispersive X-ray spectra (EDS) were acquired from Phillips XL 30 FEG-SEM (Phillips, Netherlands).TEM images, high-resolution transmission electron microscope (HRTEM) images and selected area electron diffraction (SAED) patterns were analyzed using a JEM-2100 (JEOL, Japan). XPS was acquired on a ThermoESCALAB250 spectrometer equipped with a monochromtized Al K*α* excitation source (*hv*=1486.6 eV). The Brunauer-Emmett-Teller (BET) surface area and pore structures were tested by nitrogen adsorption-desorption analysis using a ASAP-2020 apparatus (Micromeritics, USA).

2.3 Electrochemical measurements

Work electrodes were produced by coating a slurry mixture of $CuCo_2S_4$ nanoparticles (active material), carbon black (Super-P) and sodium carboxy methyl cellulose (CMC) (with a mass ratio of 7:2:1) onto a Cu foil. A lithium foil was used as the counter electrode. The value of mass loaded on the area was 0.68 mg cm^{-2}. The electrolyte was a solution of 1 M $LiPF_6$ in mixed solvents of ethylene carbonate (EC) and diethyl carbonate (DEC) with a volume ratio of 1:1. Electrochemical measurements were conducted by coin-type cells (CR2032) which were assembled in an argon filled glove box (Dellix, China). Galvanostatic charge-discharge tests were carried out on a battery tester (Land CT2001A, China) in a voltage of 0.005-3V at various current densities. The cyclic voltammetry (CV) measurements were carried out in a potential window from 0.005 to 3.0 V at a scan rate of 0.1 mV s^{-1} by an electrochemical workstation CHI 660B (Shanghai, China). Electrochemical impedance spectroscopy (EIS) was performed on an electrochemical workstation CHI 660D (Shanghai, China) in a frequency range from 0.1 Hz to 1.0×10^5 Hz.

3. Results and discussion

A representative XRD pattern of the as-prepared $CuCo_2S_4$ nanoparticles was shown in Fig. 1a. All the diffraction peaks showed the characteristic reflections of the cubic phase and were indexed to (022), (113), (004), (224), (115) and (044) planes of a carrollite-type $CuCo_2S_4$ (JCPDS card no. 42-1450). No obvious peak on impurity or contaminant had been detected, which indicated a successful synthesis of $CuCo_2S_4$ by the solvothermal method. Estimated from the full width at half maximum (FWHM) of diffraction peaks recorded at normal incidence and using the Debye-Scherer's formula $D_{hkl}=k\lambda/(\beta\cos\theta)$(where k is the Scherer constant, λ is the incident X-ray wavelength, β is the FWHM of diffraction peak, θ is the diffraction angle) [23], the average crystallite size of the as-prepared $CuCo_2S_4$ nanoparticles was calculated to be 15.8 nm. Broadening of the diffraction peaks also indicated that the sample had small grain sizes.

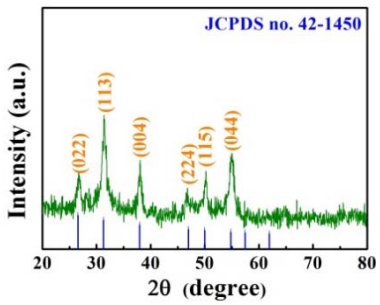

Fig. 1.Representative XRD pattern of the as-prepared $CuCo_2S_4$ nanoparticles

SEM and TEM were used to view morphologies of the as-prepared $CuCo_2S_4$ nanoparticles. As shown in Fig. 2a and 2b, the samples look like loosely packed agglomerations which was composed of a great number of irregular nanoparticles. The visible particle sizes were comparable with the calculated value of 15.8 nm from XRD result. More crystal details of $CuCo_2S_4$ nanoparticles were investigated by HRTEM (Fig. 2c) and SAED (Fig. 2d). The distances between adjacent lattice fringes were measured at about 5.49, 2.86, 2.37 and 1.82 Å, which respectively corresponded to the (111), (113), (004) and (115) planes of cubic $CuCo_2S_4$ (Fig. 2c). The calibration diffraction spots in the SAED image (Fig. 2d), suggesting the polycrystalline characteristics, were in good accordance with the HRTEM and XRD results.

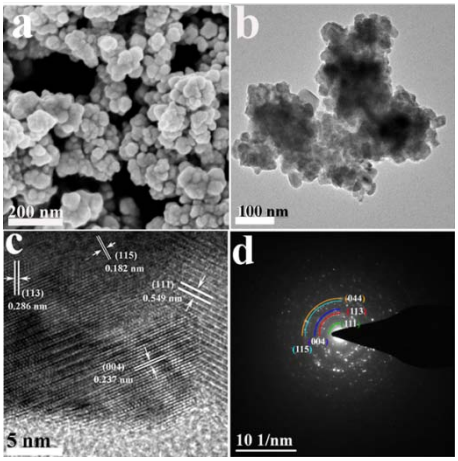

Fig. 2. (a) SEM, (b) TEM, (c) HRTEM, and (d) SAED images of the as-prepared $CuCo_2S_4$ nanoparticles

Compositions of the as-prepared $CuCo_2S_4$ nanoparticles were firstly analyzed by EDS. The molar ratio of Cu:Co:S was detected to be 1:2.21:3.59, which approaches to the integer value of 1:2:4 for $CuCo_2S_4$.XPS was carried out to obtain the information about chemical states and surface compositions of the elements in the as-prepared $CuCo_2S_4$ nanoparticles (Fig.3). The typical survey XPS spectrum in Fig.3a indicated the presence of Cu, Co, and S elements in the sample. The peaks of O and C elements might come from H_2O, O_2, or CO_2 adsorbed on the surface of the sample and adventitious hydrocarbon from XPS instrument itself[24]. Fig.3b showed the binding energies of Cu $2p_{3/2}$ and Cu $2p_{1/2}$ peaks at 932.6 and 952.6 eV, corresponding to the typical values of Cu (Ⅱ) [2, 24]. As shown in Fig.3c, the high resolution XPS spectrum of Co element contained four peaks. Among them, two strong peaks at 781.1 eV and 794.1 eV could be attributed to the existence of Co^{3+}, while the other two weak peaks at 779.1 eV and 797.1 eV could be ascribed to Co^{2+}, which indicated the coexistence of Co^{3+} and Co^{2+} in the sample [17]. There might also exist a shakeup satellite peak at 803.1 eV. Fig.3d showed the XPS spectrum of S energy region. Three peaks at 161.4, 162.5 and 168.8 eV were ascribed to $2p_{1/2}$ and $2p_{3/2}$core level of S^{2-} in $CuCo_2S_4$, as well asSO_4^{2-} sulfur, respectively[2, 25].The existence of SO_4^{2-} indicated that sulfur species on the sample's surface was partly oxidized in air. According to the results of XPS analysis, the near surface of the sample contained Cu^{2+}, Co^{2+}, Co^{3+} and S^{2-}.

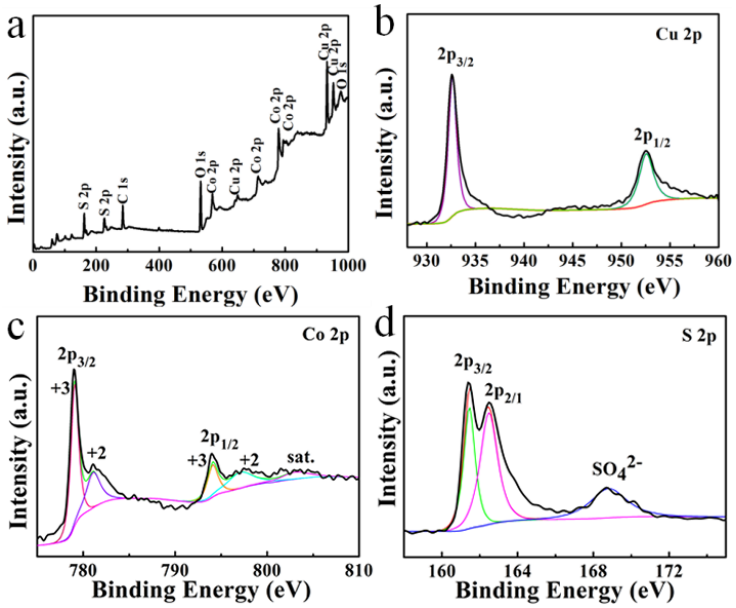

Fig.3. a)A typical survey XPS spectrum, and high resolution XPS spectra of b) Cu, c) Co and d) S elements of the as-prepared $CuCo_2S_4$ nanoparticles

Electrochemical performances of the as-prepared $CuCo_2S_4$ nanoparticles were firstly evaluated by CV in a voltage window of 0.005-3.0 V at a scan rate of 0.1 mV s^{-1} which could be described as the following equations.

$$CuCo_2S_4 + 8Li^+ + 8e^- \leftrightarrow Li_2S + Co + Cu \quad (1)$$

$$Cu + Li_2S \leftrightarrow CuS + 2Li^+ + 2e^- \quad (2)$$

$$Co + Li_2S \leftrightarrow CoS + 2Li^+ + 2e^- \quad (3)$$

$$CoS + 1/3Li_2S \leftrightarrow 1/3Co_2S_3 + 2/3Li^+ + 2/3e^- \quad (4)$$

$$Cu + Co + Li_2S \leftrightarrow Cu + Co + 2Li^+ + 2e^- + S \quad (5)$$

As shown in Fig.4a, during the first cathodic scan, the irreversible shoulder peak at 1.0 V was attributed to the formation of solid electrolyte interphase (SEI) layer and reduction of $CuCo_2S_4$.[10] The peak at 1.25 V corresponded to the initial insertion of Li-ions to form Li_2S (Eq. 1).[26] After the first cycle, two pairs of currents peaks, which were associated with the two-step lithiation/delithiation processes, could be observed. The cathodic peak at 1.25 V moved to 1.3V and three peaks at 1.6, 1.8 and 2.1 V appeared, which agreed well with the kinetics of a multistep conversion from elemental sulfur to polysulfides and then to Li_2S.[27] The peaks at 2.1 V and 1.3 V were assigned to the lithiation process of Cu (Π) and Co (Π) or Co (ⅢⅠ); The peaks at 1.6 V and 1.8 V were attributed to decomposition of lithiated electrodes toward stable phase Cu metal, Co metal and Li_2S (Eq. 2, 3, and 4).[2, 7, 28-30] For the anodic sweep, the peaks at 2.0 V and 2.3 V were relative to oxidation of Li_2S into sulfur as well as formation of Li-ions (Eq. 5).[28] From the third cycle on, positions of both anodic and cathodic peaks were nearly overlapped, which exhibited a good reversibility of the electrodes.

Discharge/charge voltage profiles of the as-prepared $CuCo_2S_4$ nanoparticle electrodes with in a potential range of 0.005-3.0V at a current density of 100 mA g^{-1}were shown in Fig. 4b. In initial discharge process, two voltage plateaus at 1.00 and 1.25 V were observed. The plateau at 1.0 V was related to formation of SEI films on the electrode surfaces, and the plateau at 1.25 V corresponded to the initial insertion of Li-ions to form Li_2S. In the subsequent cycling, the plateau at 1.0 V disappeared and the plateau at 1.25 moved to 1.3V. Meanwhile, the plateau at 1.6, 1.8 and 2.1 V were observed, which implied gradual changes of electrochemical reactions.[2] For the charge process of the electrodes, the voltage plateaus at about 2.0 and 2.3V were ascribed to the de lithiation process. From the 50^{th} cycles, both the discharge and charge plateaus of the electrodesfaded, which was indicative to the capacity fading in the subsequent cycles.

As shown in Fig.4c, the initial discharge/charge capacities of the electrode were 945.8 and 878.8 mAh g^{-1} at a current density of 100 mA g^{-1}, which indicated an initial coulombic efficiency of 93%. The capacity loss in the first cycle could be ascribed to the irreversible formation of SEI layers on the surface of the electrode due to the electrolyte decomposition [2, 31,32]. After the initial cycle, the electrode exhibited a highly stable cyclability and high coulombic efficiencies over 98%. It was observed that the reversible capacity of $CuCo_2S_4$ decreased to 836.8 mAh g^{-1}at a current density of 100 mA g^{-1}at the first 10 cycles, and then gradually increased to a value as high as 1166.2 mAh g^{-1}after 160 cycles. The behavior of “overcapacity” (the increasing reversible capacity with cycling) may be due to the reversible growth of an electrochemically gel-like polymer layer at the surface of $CuCo_2S_4$ nanoparticle electrode.[26, 32, 33] In this work, the anode material of $CuCo_2S_4$ nanoparticles exhibited a highspecific capacity and an excellent stability at a current density of 100 mA g^{-1},which were superior to most of copper-based sulfides or cobalt-based sulfides, *e.g.*,CuS nanowire bundles (550 mAh g^{-1}after 90 cycles),[6] Cu_2S nanowire (290 mAh g^{-1} after 30 cycles),[5] flower-like $Co_{1-x}S$ (485 mAh g^{-1} after 150 cycles),[32] worm-like CoS_2 (883 mAh g^{-1} after 100 cycles),[7] Co_9S_8 hollow sphere (255 mAh g^{-1} after 100 cycles),[34] cabbage-like Cu_2SnS_3(621 mAh g^{-1} after 50 cycles),[13] $NiCo_2S_4$ hollow spheres (900 mAh g^{-1} after 10 cycles),[14] porous Cu_2ZnSnS_4 films (750 mAh g^{-1} after 55 cycles).[35]

Fig.4d showed rate capacity of the electrode at various current densities of 100, 200, 500, 1000 and 2000 mA g^{-1}. The discharge capacities at such rates were 945.8, 848.5, 789.6, 509.7 and 305.1 mAh g^{-1}, respectively. It retained a specific capacity of 668.6 mAh g^{-1} when the rate returned to 100 mA g^{-1} after 60 cycles. It’s noted that electrode capacities were strongly affected by the current rate. The reversible capacities decreased slowly at the current densities of 100, 200 and 500

mA g^{-1}. But to our disappointment, when the rate increased to 1000 or 2000 mA g^{-1}, the electrode capacities dropped dramatically, which may be resulted from a structural change of $CuCo_2S_4$ nanoparticles and pulverization of electrodes during the conversion reaction.[36, 37]

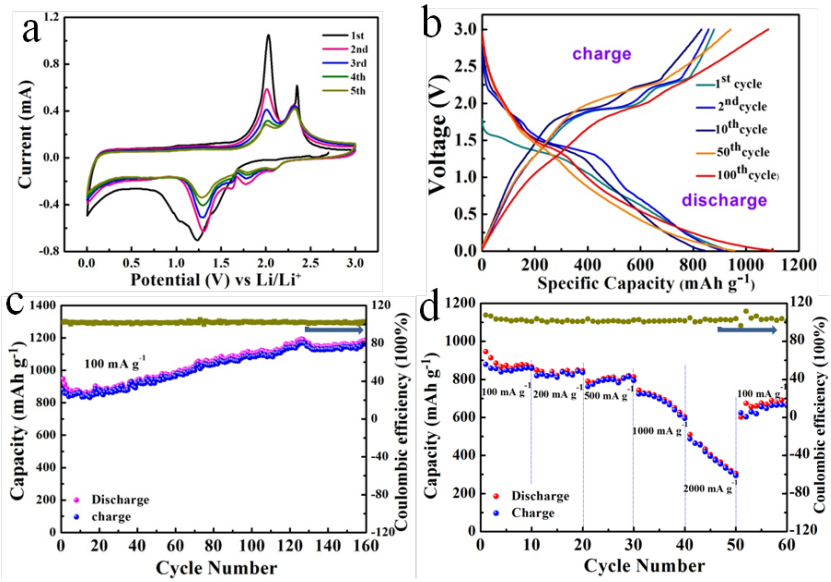

Fig.4.The as-prepared $CuCo_2S_4$ nanoparticle electrodes.(a) CV curves at a scan rate of 0.1 mV s^{-1}. (b) Voltage profiles at a current density of 100 mA g^{-1}. (c) Cycling stability at a current density of 100 mA g^{-1}. (d) Rate performanceat the current densities of100, 200, 500, 1000, 2000 and 100 mA g^{-1}.

To further understand the electrochemical behavior, $CuCo_2S_4$ nanoparticle electrodes were investigated by EIS. Fig.5 showed the representative Nyquist plots of the same battery recorded at the open circuit potential (OCP) and after 100 cycles at a current density of 100 mA g^{-1}. The equivalent circuit model in the inset was used to analyze the curves. In this model, the resistance associated with the SEI film and the electrode-electrolyte interface were represented by R_f and R_{ct}, respectively. CPE dl was the constant phase elements associated with the SEI film and electrode-electrolyte interface, and Z_W represented Warburg impedance corresponding to the Li-ion diffusion process.[9] It was found that R_f and R_{ct} at OCP (2.61 and 181.2 Ω) were significantly higher than that after 100 cycles (1.85 and 82.9 Ω), which indicated an improvement of the electrode conductivity during the cycling processes.

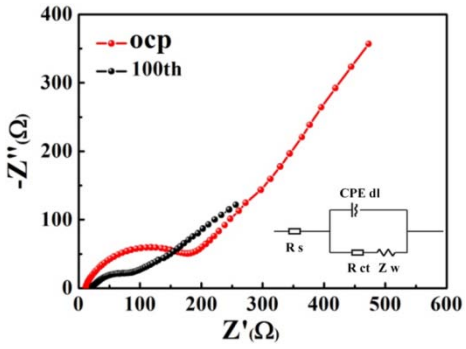

Fig.5. Nyquist plots of the same battery recorded at OCP and after 100 cycles.

4. Conclusions

To summarize, ternary $CuCo_2S_4$ nanoparticles had been synthesized by a one-pot solvothermal method. XRD results indicated the polycrystalline, cubic phase nature with an average crystallite size of 15.8 nm. SEM and TEM images viewed the loosely packed samples agglomerated by irregular nanoparticles. As a new anode material, the as-prepared $CuCo_2S_4$ nanoparticle electrodes showed an excellent specific capacity of 878.8 mAh g^{-1}at a current density of 100 mA g^{-1}in the initial charge process, and then gradually reached as high as 1166.2 mAh g^{-1} after 160 cycles. Therefore, the present results suggested that $CuCo_2S_4$ nanoparticles hold a great potential for using as an anode material for LIBs.

Acknowledgements

This work was financially supported by the NNSF of China (51402242, 21275119, 51473136, 21575116).

References

[1] X. Rui, H. Tan, Q. Yan, Nanoscale **6**, 9889(2014).
[2] C.Feng, L.Zhang, M.Yang, X.Song, H.Zhao, Z.Jia, K.Sun, G.Liu, ACS Applied Materials & Interfaces **7**, 15726(2015).
[3] Y.Liu, B.Jin, Y. F.Zhu, X. Z.Ma, X. Y.Lang, International Journal of Hydrogen Energy **40**, 670**(**2015).
[4] X.Meng, S. C.Riha, J. A.Libera, Q.Wu, H.-H.Wang, A. B. F.Martinson, J. W. Elam, Journal of Power Sources **280**, 621(2015).
[5] C.-H.Lai, K.-W.Huang, J.-H.Cheng, C.-Y.Lee, B.-J.Hwang, L.-J.Chen, Journal of Materials Chemistry **20**, 6638(2010).
[6] C.Feng, L.Zhang, Z.Wang, X.Song, K.Sun, F.Wu, G.Liu, Journal of Power Sources, **269**, 550(2014).
[7] R.Jin, L.Yang, G.Li, G.Chen, Journal of Materials Chemistry A **3**, 10677(2015).
[8] D.He, D.Wu, Gao, J.; Wu, X.; Zeng, X.; Ding, W. Flower, Journal of Power Sources **294**, 643(2015).
[9] Q. Wang, L.Jiao, H. Du, Y.Si, Y.Wang, H.Yuan, Journal of Materials Chemistry, **22**, 21387(2012).
[10] Y.Zhou, D.Yan, H.Xu, S.Liu, J.Yang, Y.Qian, Nanoscale **7**, 3520(2015).
[11] N.Mahmood, C.Zhang, J.Jiang, F.Liu, Y.Hou, Chemistry – A European Journal, **19**, 5183**(**2013).
[12] Q.Wang, L.Jiao, Y.Han, H.Du, W.Peng, Q.Huan, D.Song, Y.Si, Y.Wang, H.Yuan, The Journal of Physical Chemistry C **115**, 8300(2011).
[13] B.Qu, H.Li, M.Zhang, L.Mei, L.Chen,Y. Wang, Q.Li, T.Wang, Nanoscale **3**, 4389**(**2011).
[14] R. Jin, D.Liu, C.Liu, G. Liu, RSC Advances **5**, 84711(2015).
[15] X.Tang, X.Yao, Y.Chen, B.Song, D.Zhou, J.Kong, C.Zhao, X.Lu, Journal of Power

Sources **257**, 90(2014).
[16] J.Lin, J.Guo, C.Liu, H. Guo, ACS Applied Materials & Interfaces **7**, 17311(2015)
[17] F.Zhu, H.Xia, T.Feng, Materials Technology **30**, A53(2015).
[18] Q. Su, J.Xie, J.Zhang, Y.Zhong, G.Du,B. Xu, ACS Applied Materials & Interfaces **6**, 3016**(**2014).
[19] J. Tang, Y.Ge, J.Shen, M. Ye, Chemical Communications **52**, 1509(2016).
[20] S. E.Moosavifard, S.Fani, M. Rahmanian, Chemical Communications **52**, 4517(2016).
[21] J.Shen, J.Tang, P.Dong, Z.Zhang, J.Ji, R.Baines, M. Ye, RSC Advances **6**, 13456(2016).
[22] L.Nie, H.Wang, Y.Chai, S.Liu, R.Yuan, RSC Advances **6**, 38321(2016).
[23] S.Rabaoui, H. Dahman, S.Dekhil, K.Omri, A.Alyamani, L.El Mir, J Mater Sci: Mater Electron **26**, 8588(2015).
[24] J.Zhang, J.Yu, Y.Zhang, Q.Li, J. R. Gong, Nano Letters **11**, 4774(2011).
[25] L.-L.Feng, G.-D.Li, Y.Liu, Y.Wu, H.Chen, Y.Wang, Y.-C. Zou, D.Wang, X. Zou, ACS Applied Materials & Interfaces **7**, 980(2015).
[26] Z. X.Huang, Y.Wang, J. I.Wong, W. H.Shi, H. Y.Yang, Electrochimica Acta **167**, 388(2015).
[27] U. K.Sen, S. Mitra, ACS Applied Materials & Interfaces **5**, 1240 (2013).
[28] J.Cheng, Y.Pan, J.Zhu, Z.Li, J.Pan, Z.Ma, Journal of Power Sources **257**, 192(2014)
[29] Q.Wang, R.Zou, W.Xia, J.Ma, B.Qiu, A.Mahmood, R.Zhao, Y.Yang, D.Xia, Q. Xu, Small **11**, 2511(2015).
[30] D.-H.Ha, T.Ly, J. M.Caron, H.Zhang, K. E.Fritz, R. D. Robinson, ACS Applied Materials & Interfaces **7**, 25053(2015).
[31] W.Zhou, J.-L.Zheng, Y.-H.Yue, L.Guo, Nano Energy **11**, 428 (2015).
[32] S.Liu, J.Wang, J.Wang, F.Zhang, F.Liang, L.Wang, CrystEngComm **16**, 814(2014).
[33] R. Wu, D. P.Wang, X.Rui, B.Liu, K.Zhou, A. W. K.Law, Q.Yan, J. Wei, Z.Chen, Advanced Materials **27**, 3038(2015),
[34] R.Jin, J.Zhou, Y.Guan, H.Liu, G. Chen, Journal of Materials Chemistry A **2014**(2), 13241(2015).
[35] X.Yin, C.Tang, M. Chen, S.Adams, H.Wang, H.Gong, Journal of Materials Chemistry A **1**, 7927(2013).
[36] D. H.Youn, C.Jo, J. Y.Kim, J.Lee, J. S.Lee, Journal of Power Sources **295**, 228(2015).
[37] J.Xiao, X.Wang, X.-Q.Yang, S.Xun, G.Liu, P. K.Koech, J.Liu, J. P. Lemmon, Advanced Functional Materials **21**, 2840(2011).